Eur. J. Mineral., 38, 169–177, 2026
https://doi.org/10.5194/ejm-38-169-2026

European Journal of Mineralogy
Open Access

Friisite, $Pb_8Al_3Si_8O_{27}Cl_3$, a new mineral with a polysomatic relation to jagoite, from Långban, Sweden

Dan Holtstam[1], **Fernando Cámara**[2], **and Andreas Karlsson**[1]

[1]Department of Geosciences, Swedish Museum of Natural History, P.O. Box 50007, 10405 Stockholm, Sweden
[2]Dipartimento di Scienze della Terra 'A. Desio', Università degli Studi di Milano,
Via Luigi Mangiagalli 34, 20133, Milano, Italy

Correspondence: Dan Holtstam (dan.holtstam@nrm.se)

Received: 11 December 2025 – Revised: 11 March 2026 – Accepted: 13 March 2026 – Published: 2 April 2026

Abstract. Friisite, ideally $Pb_8Al_3Si_8O_{27}Cl_3$, is a new mineral discovered in a museum sample from the Långban mine in Värmland, Sweden. It occurs as subhedral, flaky grains up to 150 µm in size, forming aggregates within a medium-grained skarn matrix and contiguous to jagoite. Both are associated with melanotekite, aegirine–augite, albite, baryte, fluorapophyllite-K, margarosanite, alamosite, native lead, a serpentine group mineral, and a wickenburgite-like mineral. Friisite is white to colorless with a white streak and sub-adamantine luster. The mineral is transparent and does not fluoresce under UV light. It is brittle, with an uneven fracture and perfect cleavage on {001}. Mohs hardness is 4–5 (by analogy with jagoite). The calculated density is 5.54(1) g cm^{-3}. Optically, friisite is non-pleochroic and uniaxial (–). Point analyses by means of an electron microprobe using wavelength-dispersive spectroscopy resulted in an empirical formula (based on 30 O+Cl): $(Pb_{7.89}Na_{0.11}Ca_{0.08})_{\sum=8.08}(Al_{2.19}Si_{0.31}Fe^{3+}_{0.20}Zn_{0.13}Mn^{2+}_{0.11})_{\sum=2.94}Si_8O_{27.02}Cl_{2.98}$. Friisite is hexagonal, $P\bar{6}2c$ (#190), with unit-cell parameters $a = 8.5955(1)$ Å, $c = 23.4092(2)$ Å, and $V = 1497.82(4)$ Å^3 for $Z = 2$. The eight strongest powder X-ray diffraction lines are [d, Å (I_{rel}) (hkl)]: 5.848 (31) (004), 5.375 (20) (103), 4.040 (96) ($\bar{1}\bar{1}2$, 112), 3.680 (40) (201), 3.463 (100) (114), 2.886 (21) (116), 2.795 (20) ($\bar{2}\bar{1}1$), and 2.4828 (35) (300). Friiste is a phyllosilicate and forms a polysomatic series with jagoite characterized by a layer sequence of SiO_4 tetrahedra (T) and metal octahedra (O) between double layers (*) corresponding to *TOT*, whereas jagoite is described as *TOTOT*. Friisite forms from transformation of melanotekite or barysilite in the presence of albite and a Cl-enriched fluid at relatively high a_{SiO_2}. The mineral (IMA2024-047) is named in honor of Danish mineralogist Henrik Friis (b. 1977), professor at the Natural History Museum, University of Oslo, Norway.

1 Introduction

Lead silicates represent a chemically and structurally diverse category of rare minerals (with about 50 species known so far) that crystallize under specific geological conditions, typically in Pb-rich skarn environments or oxidized zones of polymetallic ore deposits. These minerals, characterized by the incorporation of Pb^{2+} ions, with frequently stereochemically active lone-pair electrons, and $(SiO_4)^{4-}$ units within their crystal structures, often exhibit complex compositions and unusual structural motifs, reflecting the variable coordination chemistry of lead and the polymerization behavior of silica tetrahedra. Notable species include exotica like alamosite, larsenite, ganomalite, barysilite, the kentrolite–melanotekite series, and wickenburgite. The study of lead silicates potentially provides valuable insights into mineral formation processes across a range of temperatures, particularly concerning the mobility of lead in nature and, by extension, the technogenic environment.

During an investigation of the rare mineral jagoite, $Pb_{11}Fe_5Si_{12}O_{41}Cl_3$, and its paragenesis (Holtstam et al., 2025), from the Långban mine in Värmland, Sweden, a new, structurally related lead silicate was discovered. It is named "friisite" (IMA2024-047) in honor of the Danish mineralogist Henrik Friis (b. 1977), professor at the Natural History Museum, University of Oslo, Norway, in recognition of his

significant contributions to Nordic (including Greenlandic) mineralogy. It must not be confused with "frieseite", an obsolete name and near-homophone, referring to a mixture of sulfide minerals (Ondruš et al., 2003). The mineral symbol is "Fii". The holotype material is housed in the type mineral collection of the Department of Geosciences, Swedish Museum of Natural History, Box 50007, SE-10405 Stockholm, Sweden, under collection no. GEO-NRM #19610234.

2 Occurrence

The Långban Fe–Mn–(Ba–As–Pb–Sb–W–Be–B) deposit, located in the Filipstad district (lat 59°51′ N, long 14°15′ E), was mined continuously from 1711 to 1972 for iron (hematite–magnetite) and manganese (braunite–hausmannite) ores, as well as dolomitic marble. The syngenetic, carbonate-hosted Långban-type deposits of the Bergslagen ore region (Moore, 1970) are interpreted to have formed at ca. 1.9 Ga from hydrothermal–volcanogenic fluids in a shallow submarine setting (Boström et al., 1979; Holtstam and Mansfeld, 2001). These deposits occur within a supracrustal sequence dominated by rhyolitic volcanic and volcaniclastic rocks that, together with the ores and interbedded dolomitic carbonate horizons, experienced regional metamorphism under amphibolite-facies conditions. Subsequent thermal overprinting occurred during the emplacement of Svecokarelian magmatic intrusions between 1.87 and 1.75 Ga (Stephens and Jansson, 2020). Långban is internationally renowned for its exceptional mineral diversity (Holtstam and Langhof, 1999) and significance as a type locality, with 81 IMA-approved mineral species currently recognized (including friisite; see https://www.mindat.org/, last access: 24 February 2026).

In a comprehensive geological and mineralogical study of the Långban deposit, Magnusson (1930) delineated four major paragenetic stages, denominated A, B, C, and D. The earliest, A and B, are associated with ore and skarn formation, with stage B encompassing the regional metamorphic peak (at approximately 600 °C and 0.3 GPa; Skelton et al., 2018). The later periods, C and D, correspond to mineral formation in vugs and fissures, respectively, under progressively lower temperature and pressure conditions.

The new mineral (Figs. 1 and 2) was found in a museum specimen of jagoite with heterogeneous skarn associated with hematite ore, collected from the *Canberra* stope at 220 m depth in the mine and provided by John Gustaf Herman Weslien in 1961. This specimen also contains melanotekite, aegirine–augite, jagoite, albite, baryte, fluorapophyllite-K, margarosanite, alamosite, native lead, a serpentine group mineral, and a wickenburgite-like mineral. Mineral identification was mainly done using energy-dispersive X-ray spectroscopy under the scanning-electron microscope (FEI Quanta 650 field emission gun scanning-electron microscope fitted with a back-scattered electron detector and an 80 mm^2 X-Max^N Oxford Instruments energy dispersion micro-analyzer) on polished sections embedded in epoxy resin.

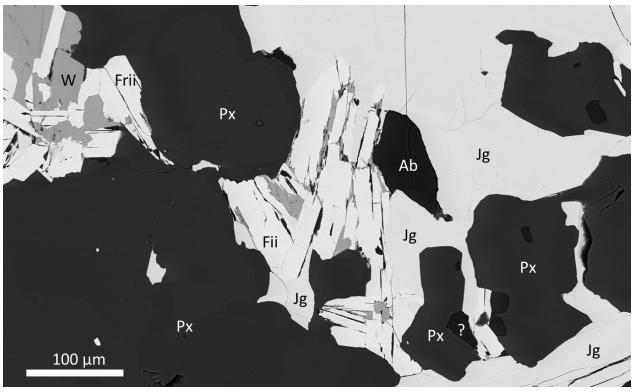

Figure 1. Back-scattered electron image of friisite (Fii) with pyroxene (Px), albite (Ab), jagoite (Jg), and a wickenburgite-like mineral (W). The question mark is possibly a serpentine mineral. Sample no. GEO-NRM #19610234.

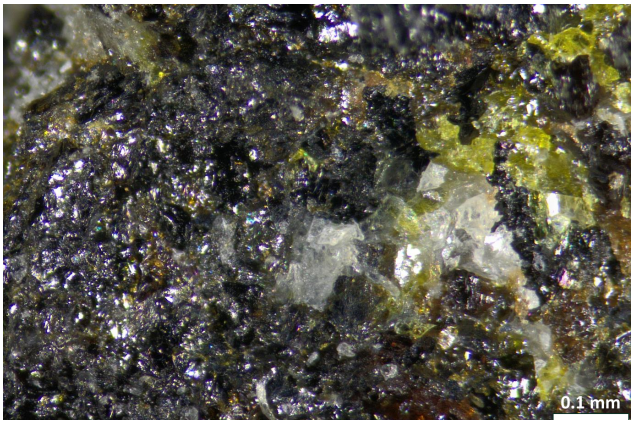

Figure 2. Color image of the type specimen, with friisite (white), jagoite (yellow), aegirine–augite (brown), and melanotekite (black). Sample no. GEO-NRM #19610234.

3 Physical and optical description

Friisite occurs as subhedral, flaky grains up to 150 µm in size, forming aggregates within a medium-grained skarn matrix and contiguous to jagoite. It is white to colorless with a white streak and exhibits a sub-adamantine luster. The mineral is transparent and does not fluoresce under UV light. It is brittle, with an uneven fracture and perfect cleavage on {001}; no parting was observed. Based on analogy with jagoite, the Mohs hardness is estimated to be 4–5. The density could not be measured due to the small grain size and an expected value exceeding the limits of available heavy liquids. The calculated value is 5.54(1) g cm^{-3}, derived from the empirical formula and single-crystal X-ray diffraction data (see be-

Table 1. Chemical data (in wt %) for friisite.

Constituent	Mean	Range	2σ	Reference material
Na_2O	0.14	0.10–0.17	0.05	jadeite
Al_2O_3	4.42	3.27–4.87	1.10	almandine
SiO_2	19.80	19.10–20.38	0.93	almandine
Cl	4.19	3.99–4.42	0.30	tugtupite
CaO	0.19	0.16–0.26	0.07	bustamite
MnO	0.31	0.17–0.57	0.30	rhodonite
Fe_2O_3	0.63	0.45–0.91	0.33	hematite
ZnO	0.42	0.34–0.61	0.18	willemite
PbO	69.83	69.10–71.16	1.50	crocoite
$O \equiv Cl$	−0.94			
Total	98.98	98.26–99.99		

low). Optically, friisite is non-pleochroic and uniaxial negative, with a calculated average refractive index of $n = 1.88$ using Gladstone–Dale constants (Mandarino, 2007).

4 Chemical composition

The composition of friisite was determined with electron microprobe analyses (EMPAs) collected with an AZtecWave wavelength–dispersion (WDS) system attached to an FEI Quanta 650 field emission scanning-electron microscope at 20 kV and 14 nA, with a working distance of 10 mm. The polished sample surface was carbon-coated to 20 nm thickness prior to analysis. The mineral reference materials (SPI 53) used and the analytical results are shown in Table 1. The number of spot analyses was six. Mg, Sb, and Br concentrations in the sample were close to or below the detection limit with this method. Neither H_2O nor CO_2 was indicated in structural or spectroscopic data for the mineral vide infra, and these are thus not considered in the formulae.

The empirical formula calculated from the EMPA data, normalized on a basis of 30 anions (O + Cl), is $(Pb_{7.89}Na_{0.11}Ca_{0.08})_{\sum=8.08}(Al_{2.19}Si_{0.31}Fe^{3+}_{0.20}Zn_{0.13}Mn^{2+}_{0.11})_{\sum=2.94}Si_8O_{27.02}Cl_{2.98}$. The analyzed crystal is heterogeneous with respect to some metal components, where the Al_2O_3 content is negatively correlated to Fe_2O_3+MnO+ZnO (linear $R^2 = 0.95$).

The simplified formula is $(Pb,Na,Ca)_8(Al,Si,Fe,Zn,Mn)_3Si_8O_{27}Cl_3$, whereas the ideal formula is $Pb_8Al_3Si_8O_{27}Cl_3$, which would require PbO 71.38 %, Al_2O_3 6.11 %, SiO_2 19.22 %, Cl 4.25 %, $Cl \equiv O$-0.96 %, and a sum of 100.00 wt %.

5 Raman micro-spectroscopy

Micro-Raman spectra were obtained at Laboratorio di Mineralogia Sperimentale "Fiorenzo Mazzi", Università di Pavia, with a Horiba LabRAM HR Evolution spectrometer equipped with an Olympus BX41 confocal microscope and a

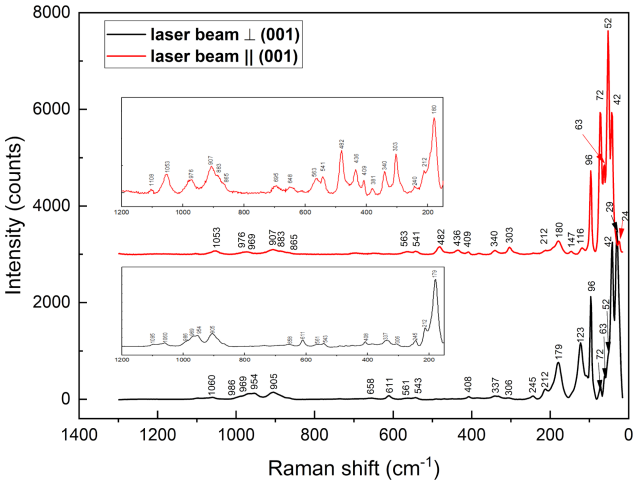

Figure 3. Micro-Raman spectra of friisite with laser beam perpendicular to (001) and with laser beam parallel to (001), with insets enlarged from 150 to 1200 cm^{-1}.

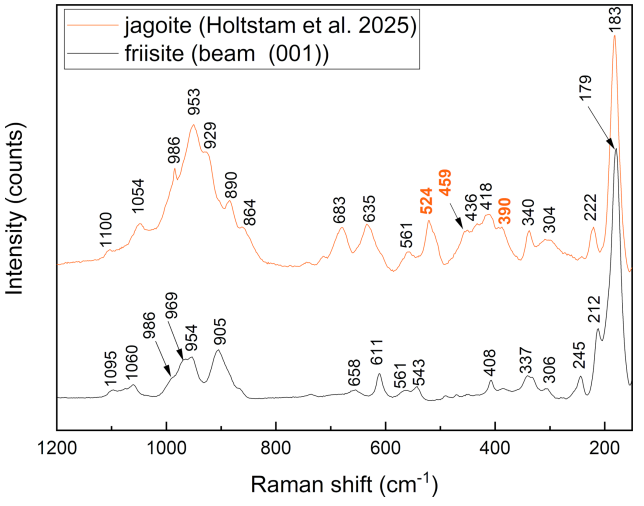

Figure 4. Micro-Raman spectra of friisite and comparison with jagoite (from Holtstam et al., 2025).

Symphony BIDD detector and a solid-state (YAG) 532 nm laser focused to a 1 µm diameter spot (power of 2.06 and 5.02 mW). Measurements were done with a 100×VIS objective, 600 groves mm^{-1} grating, and spectra calibrated against pure silicon. The acquisition time was 15 s in 10 separate accumulations. Spectra were processed using LabSpec 6 software suite by Horiba for background subtraction and peak fitting. The spectra (Fig. 3) have distinct common features with that of jagoite (Holtstam et al., 2025): very intense bands at values < 250 cm^{-1} and weaker bands up to 1100 cm^{-1}. No Raman bands are observed at > 1100 cm^{-1}. The spectra exhibit polarization effects that vary with crystal orientation, with one component perpendicular to and the other parallel to the (001) cleavage plane. The most intense bands are observed at 29, 42, 52, 63, 72, 96 123, 179, and ∼213 cm^{-1};

the strongest polarization effects are observed for the bands at 52, 73, and 123 cm^{-1}. Jagoite and friisite have common bands at 52, 64, 72, 96 (100 for jagoite), and 179 (183 cm^{-1} for jagoite; see Holtstam et al., 2025 and Fig. 4). This is not surprising since those modes are related to lattice vibrations and considering the fact that both minerals belong to a polysomatic series with similar types of layers in the crystal structure (see below). The two latter bands can possibly be assigned to O–Pb–O and/or Cl–Pb–Cl bending modes. In the intermediate-range (300–700 cm^{-1}) bands at ~ 306, ~ 340, ~ 406, 541, and 562 are much weaker but present in both orientations, with some other peaks showing polarization at 436 and 482 cm^{-1} (laser beam parallel to (001)) and 611 and 659 cm^{-1} (perpendicular to (001)); all of these bands are related to bending modes of SiO_4/AlO_4 groups. In the higher range (700–1200 cm^{-1}), weak bands are observed at ~ 869, ~ 885, 905, 964, ~ 970, and ~ 1060 cm^{-1}, with minor shoulders poorly defined; these are believed to be related to stretching modes of SiO_4/AlO_4 groups. Very similar band positions are observed for jagoite (Fig. 4). The only differences are bands at 390, 459, and 524 cm^{-1} for jagoite (with numbers in red in Fig. 4).

6 X-ray crystallography

6.1 Powder data

Gandolfi-type X-ray powder diffraction data were collected with $\lambda = 0.71073$ Å radiation.

The unit-cell parameters refined from the powder data, using least squares with minimization based on $Q = 1/d^2$ (Holland and Redfern, 1997), are $a = 8.599(6)$, $c = 23.379(8)$, and $V = 1497.11(4)$ $Å^3$ for $Z = 2$. The complete X-ray powder diffraction data are shown in Table 2.

Table 2. X-ray powder diffraction data (d in Å) for friisite.

I (obs)	I (calc)*	d (obs)	d (calc)*	h	k	l
	2		11.7046	0	0	2
6	6	7.47	7.4439	1	0	0
31	20	5.848	5.8523	0	0	4
20	31	5.375	5.3861	1	0	3
	2		4.6007	1	0	4
96	89	4.040	4.0344	$\bar{1}$	$\bar{1}$	2
				1	1	2
	20		3.9631	1	0	5
40	28	3.680	3.6758	2	0	1
	8		3.5469	2	0	2
100	100	3.463	3.4640	1	1	4
				$\bar{1}$	$\bar{1}$	4
6	15	3.134	3.1406	2	0	4
	26		2.9262	0	0	8
21	54	2.886	2.8887	1	1	6
				$\bar{1}$	$\bar{1}$	6
	6		2.8135	$\bar{2}$	$\bar{1}$	0
				2	1	0
20	26	2.795	2.7934	$\bar{2}$	$\bar{1}$	1
				2	1	1
	10		2.7356	2	1	2
				$\bar{2}$	$\bar{1}$	2
	8		2.7233	1	0	8
	10		2.6931	2	0	6
5	15	2.6478	2.6467	2	1	3
				$\bar{2}$	$\bar{1}$	3
	22		2.5357	$\bar{2}$	$\bar{1}$	4
				2	1	4
	8		2.4876	2	0	7
35	31	2.4828	2.4813	3	0	0
	2		2.4274	3	0	2
	3		2.4187	1	1	8
				$\bar{1}$	$\bar{1}$	8
	8		2.4116	$\bar{2}$	$\bar{1}$	5

* Calculated with Vesta (Momma and Izumi, 2011). Reflections with intensities < 2 % are omitted.

6.2 Single-crystal data

The single-crystal X-ray study was done on a 102 × 63 × 33 µm fragment using a Rigaku Oxford Diffraction XtaLAB Synergy diffractometer, equipped with a PhotonJet (Mo) X-ray source operating at 50 kV and 1 mA, with a monochromatized Mo$K\alpha$ radiation and equipped with a HyPix detector working at 62 mm from the crystal. A combination of ω scans at different values of ϕ, κ, and θ positions, with a step scan of 0.5° and exposure times of 2 and 8 s per frame, was used to maximize redundancy, data coverage, and absorption correction. A crystallographic information file (CIF) containing observed structure factors has been deposited in the Supplement. Crystal and refinement data are summarized in Table 3. Table 4 contains the atom parameters, and interatomic bond distances are reported in Table 5.

Friisite has a hexagonal (ditrigonal dipyramidal) symmetry, and the crystal structure was solved in space group $P\bar{6}2c$ (#190) by the dual-space algorithm (SHELXT, Sheldrick, 2015a) and was refined to $R1 = 1.44$ % for 2461 unique reflections using the least-square methods (SHELXL, Sheldrick, 2015b). The crystal showed a merohedral twinning on [$\bar{1}$ 0 0, 0 $\bar{1}$ 0, 0 0 1], with a twin ratio of 0.735(7) / 0.265(7).

Friisite is a sheet silicate with a double layer. Each layer of the double layer is based on the $(12^2)_3(12^3)_2$ net (Hawthorne et al., 2019). Two types of SiO_4 tetrahedra (labeled Si1 and Si2) and Al(Fe^{3+}) tetrahedra (labeled T) form the double layer generated by a class-2 oikodoméic m operation. The tetrahedra of the double layer connect in 12-membered rings (Fig. 5). The composition of the double layer is then $[Al_2Si_8O_{27}]^{16-}$. Layers of metal-bearing octahedra are sandwiched on each side (Fig. 6). The regular octahedra at the origin, occupied by Al, are connected to Si2 tetrahedra. The slightly distorted large T tetrahedra, connected in pairs via a common apical oxygen atom to link the double layer, have

Table 3. Crystal data and structure refinement.

Temperature (K)	293
Crystal system	hexagonal
Space group	$P\bar{6}2c$
a (Å)	8.59550(10) Å
c (Å)	23.4092(2) Å
Volume (Å^3)	1497.82(4) Å^3
Z	2
ρ_{calc} (g cm^{-3})	5.54
μ (mm^{-1})	44.504
$F_{(000)}$	2114.0
Crystal size (mm^3)	0.102 × 0.063 × 0.033
Radiation	Mo$K\alpha$
2Θ range for data collection (°)	3.48 to 72.776
Index ranges	$-14 \le h \le 14$, $-13 \le k \le 14$, $-38 \le l \le 38$
Reflections collected	60 680
Independent reflections	2461 [$R_{int} = 0.0500$, $R_\sigma = 0.0160$]
Data/restraints/parameters	2461/0/87
Goodness of fit on F^2	1.062
Final $R1$ indexes ($I > 2\sigma_I$)	0.0144
Final R indexes (all data)	0.0163
Largest diff. peak/hole (e Å^{-3})	1.16/ − 1.03
Flack parameter	0.000(3)

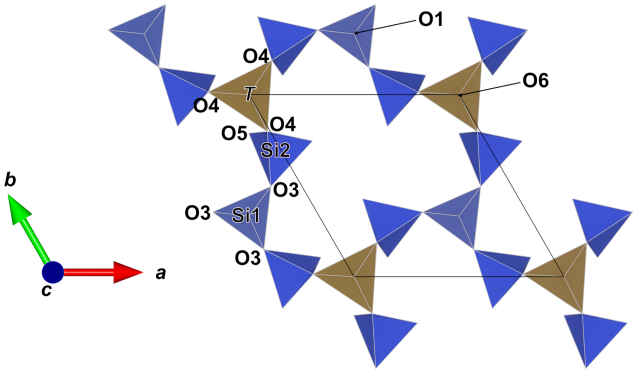

Figure 5. The 12-membered ring in the double layer of tetrahedra in friisite. Blue tetrahedra denote Si, and brown tetrahedra are Al-dominant (with Fe^{3+} and so on in solid solution). Figure obtained using Vesta 3.0 (Momma and Izumi, 2011).

mixed Al : Si : Fe : Zn : Mn occupancy. The antipathetic relation found for Al vs. Fe+Mn+Zn is mainly related to substitutions at T. This site has the largest polyhedral volume among the three four-coordinated sites in friisite.

Lead occurs in three non-equivalent positions (Pb1, Pb2, Pb3). The Pb1 position is three-coordinated to oxygen atoms and three very distant Cl atoms. The Pb2 atom is seven-coordinated and lies in the octahedral layer. Pb3 occupies voids in the double layer, where it is eight-coordinated to five O atoms and three Cl atoms, without pronounced stereo-

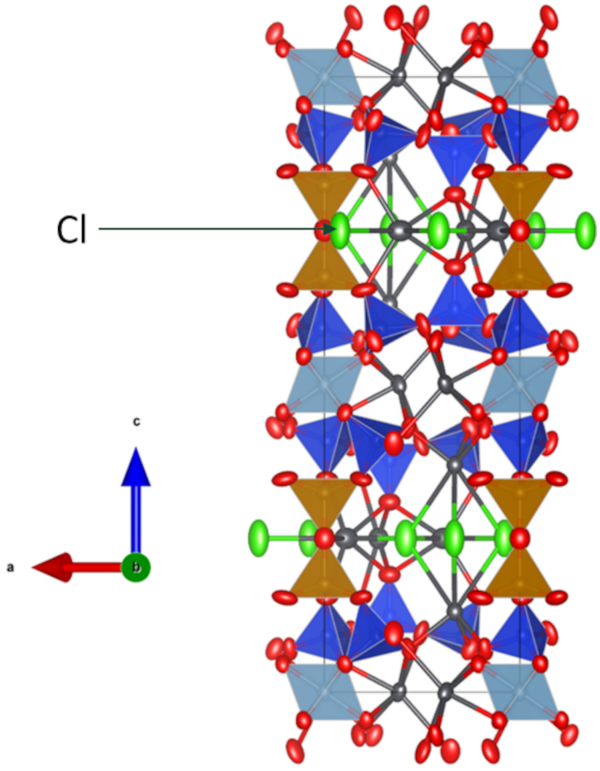

Figure 6. The crystal structure of friisite viewed along [010]. Atomic displacement parameters are shown at the 95 % probability level. Lead atoms are shown in dark gray, oxygen is shown in red, chlorine (Cl) is shown in green, and aluminum octahedra are shown in greyish blue. Tetrahedra are in brown (with Al, Fe, etc.) and blue (Si). Figure is generated with VESTA 3.0 (Momma and Izumi, 2011).

active lone-pair behavior of Pb^{2+}. This site may also host minor Na and Ca. The agreement between the refined site scattering values at the cation sites and those calculated from chemical analyses is excellent (see Table 6).

7 Discussion

7.1 Formation of friisite

Friisite is the only known mineral in the pure Pb–Al–Si–O–Cl system (bobmeyerite includes H_2O and additional cations; Kampf et al., 2013). Lead and chlorine are, in relative terms, along with Be and As, the most important elements contributing to the diversity of mineral species in the Långban deposit, with 60 Pb minerals (of which 33 are types = 55 %), 24 Cl minerals (16 types = 67 %), and 19 with Pb+Cl combined (14 types = 74 %). Jagoite is a rare mineral at the deposit, although fairly rich samples exist locally from a restricted zone in hematite ore. Friisite is very rare and only known from the type specimen. This sample is different from other jagoite specimens in that it contains more aluminum in the

Table 4. Refined fractional atomic coordinates and equivalent isotropic displacement parameters (Å^2). U_{eq} is defined as one-third of the trace of the orthogonalized U^{ij} tensor. BVS is the bond valence sum (in valence units) calculated with the parameters of Gagné and Hawthorne (2015) and Brese and O'Keeffe (1991) for bonds to O and Cl, respectively.

Site	Occupancy	x	y	z	U_{eq}	BVS
Pb1	0.979(4) Pb	1/3	2/3	0.63062(2)	0.01109(6)	1.89
Pb2	0.976(4) Pb	0	0.62042(2)	1/2	0.01342(5)	2.02
Pb3	0.937(4) Pb	0.72307(4)	0.61193(4)	1/4	0.02241(7)	1.96
Si1	1 Si	2/3	1/3	0.37711(7)	0.0085(3)	4.11
Si2	1 Si	0.73262(13)	0.71498(15)	0.40902(4)	0.0089(2)	3.97
T	0.600(6) Fe	0	0	0.32455(6)	0.0105(4)	3.02
M	1.054(16) Al	0	0	1/2	0.0064(7)	3.10
Cl	0.995(9) Cl	0.10800(3)	0.6637(3)	1/4	0.0341(6)	0.97
O1	1 O	3/3	1/3	0.3093(2)	0.0201(9)	1.91
O2	1 O	0.5699(4)	0.7451(4)	0.42978(12)	0.0137(5)	1.86
O3	1 O	0.6454(4)	0.4952(4)	0.40445(14)	0.0189(6)	2.05
O4	1 O	0.8123(5)	0.7992(5)	0.34670(12)	0.0213(7)	1.99
O5	1 O	0.8956(4)	0.7882(3)	0.45468(10)	0.0112(4)	2.08
O6	1 O	0	0	1/4	0.0194(14)	1.87

Table 5. Selected interatomic distances (Å) and bond angles for friisite.

Pb1–O2[1]	2.284(3)	Pb2–O2[3]	2.596(3)	Pb3–Cl	2.8712(19)
O2[2]	2.284(3)	O2[4]	2.596(3)	Cl[6]	2.879(2)
O2	2.284(3)	O5[5]	2.303(3)	Cl	3.409(3)
Cl	3.536(3)	O5	2.303(3)	O1	2.595(2)
Cl	3.536(3)	O3	2.990(4)	O1[7]	2.595(2)
Cl	3.536(3)	O3	2.990(4)	O4	2.659(3)
$<$Pb1–$\phi>$	2.910	O2	3.180(3)	O4[7]	2.659(3)
V (Å^3)	27.83	$<$Pb2–O$>$	2.767	O6	2.9753(3)
d.i.*	0.2152	V (Å^3)	34.77	$<$Pb3–$\phi>$	2.830
		d.i.	0.1148	V (Å^3)	38.31
M–O5[4]	1.900(3)			d.i.	0.0718
O5[3]	1.900(2)				
O5[5]	1.900(2)	Cl–Cl	3.750(5)	O4–O3–O3	147.8(2)°
O5[9]	1.900(2)	Pb1–Pb2	4.071(1)	O3–O4–O4	121.2(4)°
O5	1.900(2)	Pb2–Pb2	4.657(1)	O4–O3–O3	107.3(3)°
O5[10]	1.900(3)	Pb3–Pb3	3.798(1)	Si2–T–Si2	83.34(7)°
$<M$–O$>$	1.900			Si2–Si1–Si2	114.47(5)°
V (Å^3)	9.14			T–Si2–Si1	110.49(8)°
d.i.	0.0000				
T–O6	1.7452(15)	Si1–O1	1.588(5)	Si2–O2	1.618(3)
O4	1.751(4)	O3[8]	1.623(3)	O3	1.651(3)
O4[3]	1.751(4)	O3[6]	1.623(3)	O4	1.624(3)
O4[9]	1.751(4)	O3	1.623(3)	O5	1.616(3)
$<T$–O$>$	1.750	$<$Si1–O$>$	1.614	$<$Si2–O$>$	1.627
V (Å^3)	2.74	V (Å^3)	2.15	V (Å^3)	2.20
d.i.	0.0013	d.i.	0.0082	d.i.	0.0074

[1] *1-Y,1+X−Y,+Z*; [2] *+Y-X,1-X,+Z*; [3] *+Y,+X,1-Z*; [4] *2-Y,1+X−Y,+Z*; [5] *2-X,1-X+Y,1-Z*; [6] *1-Y,+X−Y,+Z*; [7] *+X,+Y,1/2-Z*; [8] *1+Y-X,1-X,+Z*; [9] *1+Y-X,2-X,+Z*; [10] *1-Y+X,2-Y,1-Z*. * Distortion index (Baur, 1974).

Table 6. Assignment of cations and observed and calculated site scattering values (s.s., in electrons per site) in friisite.

Atom site	Cation assignment	Observed s.s.	Calculated s.s
Si1	Si	14	14
Si2	Si	14	14
T	$Al_{0.63}Fe^{3+}_{0.07}Mn^{2+}_{0.06}Zn_{0.07}Si_{0.16}$	15.60(8)	15.85
M	$Al_{0.94}Fe^{3+}_{0.06}$	13.7(4)	13.78
Pb1	Pb	79.4(3)	82
Pb2	Pb	79.4(3)	82
Pb3	$Pb_{0.93}Na_{0.04}Ca_{0.03}$	75.5(3)	77.3

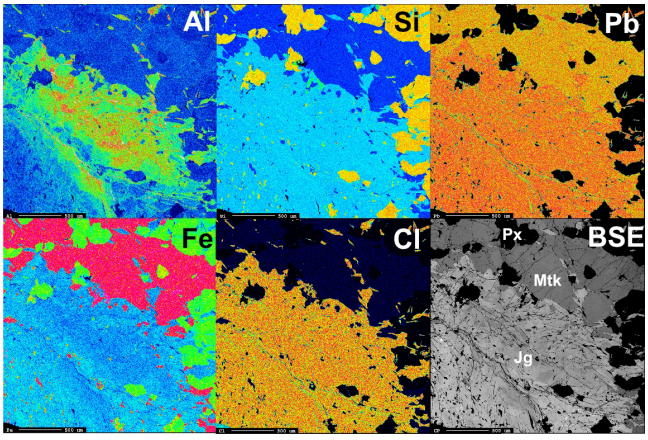

Figure 7. Elemental map of a polished section of sample GEONRM #19610234 showing the internal variation of Al versus Fe^{3+} in jagoite (Jg). Maps for Al$K\alpha$, Si$K\alpha$, Pb$M\alpha$, Fe$K\alpha$, and Cl$K\alpha$ are shown along with a back-scattered image of the same area. Other minerals shown in the map are melanotekite (Mtk) and pyroxene (Px), with composition $Ae_{33-48}Di_{67-56}$.

bulk rock, which is reflected in the presence of albite and a high but variable Al_2O_3 content in the jagoite mass (Fig. 7).

As is inferred for jagoite (Holtstam et al., 2025), friisite likely crystallized after the main skarn-forming event (post-peak metamorphism) from the transformation of earlier-formed lead silicates, melanotekite (Mtk), or barysilite (Bsl). The reactions require the presence of Al-bearing silicate (albite) and a Cl-enriched fluid at relatively high a_{SiO_2}:

$$\underset{\text{Mtk}}{4Pb_2Fe_2Si_2O_9} + \underset{\text{Ab}}{3NaAlSi_3O_8} + 3HCl(aq) \rightarrow \underset{\text{Fii}}{Pb_8Al_3Si_8O_{27}Cl_3} + 4Fe_2O_3 + 3NaOH(aq) + 9\,SiO_2(aq) \quad \text{(R1)}$$

or

$$\underset{\text{Bsl}}{Pb_8Mn(Si_2O_7)_3} + \underset{\text{Ab}}{NaAlSi_3O_8} + 5HCl(aq) \rightarrow \underset{\text{Fii}}{Pb_8Al_3Si_8O_{27}Cl_3} + 3NaOH(aq) + MnCl_2(aq) + 7SiO_2 + H_2O. \quad \text{(R2)}$$

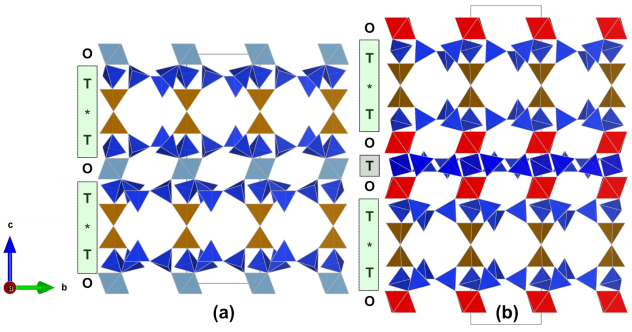

Figure 8. Comparison of the layer sequences in friisite **(a)** and jagoite (Mellini and Merlino, 1981; Holtstam et al., 2025) **(b)**. Colors are given as in Fig. 5. Cyan octahedra are Al-dominant, and red octahedra are Fe^{3+}-dominant (in jagoite). The position of the double layers is indicated with an asterisk (*).

The estimated temperature range for these reactions is 300–500 °C (between peak metamorphism conditions and the hydrothermal D stage in the deposit; see Sandström and Holtstam, 1999).

Friisite has, in part, suffered late-stage alteration during a hydrothermal episode into a wickenburgite-like phase (designated W):

$$\underset{\text{Fii}}{7Pb_8Al_3Si_8O_{27}Cl_3} + 11Ca^{2+}(aq) + Al^{3+}(aq) + 54SiO_2(aq) + 44H_2O \rightarrow \underset{\text{W}}{11Pb_3CaAl_2Si_{10}O_{27}\cdot 4H_2O} + 23Pb^{2+}(aq) + 21Cl^-(aq). \quad \text{(R3)}$$

This reaction likely took place at a lower temperature (< 300 °C) under acidic to near-neutral pH conditions. It may also have been promoted by reducing conditions, facilitating the removal of Pb precipitating as native metal.

7.2 Structural topology and relation to jagoite

Friisite has a unique composition and crystal structure but is closely structurally and chemically related to jagoite, ideally $Pb_{11}Fe_5Si_{12}O_{41}Cl_3$. Both minerals are classified as phyllosilicates and belong to the Nickel–Strunz group 09.EG. Whereas jagoite, with the unit-cell parameter $c = 33$ Å (Mellini and Merlino, 1981; Holtstam et al., 2025), has a layer sequence of SiO_4 tetrahedra (T) and metal octahedra (O) between the double layers (*) *TOTOT*, friisite has a shorter *c*-axis repeat (23 Å) corresponding to *TOT* (Fig. 8). Friisite has the precise charge arrangement $[^{Pb1}(2+)_2{}^{Pb2}(2+)_3{}^{Pb3}(2+)_3]^M(3+)[^{Si1}(4+)_2{}^{Si2}(4+)_6{}^T(3+)_2]^O(2-)_{27}{}^{Cl}(1-)_3$, and, consequently, an ideal structural formula could be written $Pb_8Al[Al_2Si_8O_{27}]Cl_3$. Jagoite can then be regarded to be an intercalation of an Fe-analogue of friisite with a hypothetical single-sheet phyllosilicate module (SSPM):

$$\underset{\text{Fe-analogue of friisite}}{Pb_8Fe^{3+}\left[Fe_2^{3+}Si_8O_{27}\right]Cl_3} + \underset{\text{SSPM}}{Pb_3Fe^{3+}\left[Fe^{3+}Si_4O_{14}\right]} = \underset{\text{jagoite}}{Pb_{11}Fe_2^{3+}\left[Fe_2^{3+}Si_8O_{27}\right]\left[Fe^{3+}Si_4O_{14}\right]Cl_3}$$

With the two modular building blocks established and given that Al can extensively substitute for Fe^{3+}, it is likely that new polysomatic members or stacking-disordered "jagoite-type" minerals can be found in geological systems similar to the Pb-rich skarns of Långban-type deposits and in anthropogenic products, like Pb smelter slags.

Data availability. A CIF is deposited in the Supplement.

Supplement. The supplement related to this article is available online at https://doi.org/10.5194/ejm-38-169-2026-supplement.

Author contributions. Conceptualization: DH. Data collection and interpretation: all authors. Paper writing: DH, with contributions from the co-authors.

Competing interests. The contact author has declared that none of the authors has any competing interests.

Disclaimer. Publisher's note: Copernicus Publications remains neutral with regard to jurisdictional claims made in the text, published maps, institutional affiliations, or any other geographical representation in this paper. The authors bear the ultimate responsibility for providing appropriate place names. Views expressed in the text are those of the authors and do not necessarily reflect the views of the publisher.

Acknowledgements. FC thanks Mateo Alvaro from the Department of Earth and Environmental Sciences of the University of Pavia for granting access to the micro-Raman at Laboratorio di Mineralogia Sperimentale "Fiorenzo Mazzi". We thank Anthony Kampf and an anonymous reviewer for their work that improved our paper.

Financial support. FC acknowledges financial support from the Italian Ministry of Education (MUR) through the project "Dipartimenti di Eccellenza 2023–2027".

Review statement. This paper was edited by Sergey Krivovichev and reviewed by Anthony Kampf and one anonymous referee.

References

Baur, W. H.: The geometry of polyhedral distortions. Predictive relationships for the phosphate group, Acta Crystallogr. B, 30, 1195–1215, https://doi.org/10.1107/S0567740874004560, 1974.

Brese, N. E. and O'Keeffe, M.: Bond-valence parameters for solids, Acta Crystallogr. B, 47, 192–197, https://doi.org/10.1107/S0108768190011041, 1991.

Boström, K., Rydell, H., and Joensuu, O.: Långban – An exhalative sedimentary deposit?, Econ. Geol., 74, 1002–1011, https://doi.org/10.2113/gsecongeo.74.5.1002, 1979.

Gagné, O. C. and Hawthorne, F. C.: Comprehensive derivation of bond-valence parameters for ion pairs involving oxygen, Acta Crystallogr. B, 71, 562–578, https://doi.org/10.1107/S2052520615016297, 2015.

Hawthorne, F. C., Uvarova, Y. A., and Sokolova, E.: A structure hierarchy for silicate minerals: sheet silicates, Mineral. Mag., 83, 3–55, https://doi.org/10.1180/mgm.2018.152, 2019.

Holland, T. J. B. and Redfern, S. A. T.: Unit cell refinement from powder diffraction data: the use of regression diagnostics, Mineral. Mag., 61, 65–77, https://doi.org/10.1180/minmag.1997.061.404.07, 1997.

Holtstam, D. and Langhof, J. (Eds.): Långban. The mines, their minerals, geology and explorers, Swedish Museum of Natural History and Raster Förlag, Stockholm, 215 pp., ISBN 9789187214882, 1999.

Holtstam, D. and Mansfeld, J.: Origin of a carbonate-hosted Fe-Mn-(Ba-As-Pb-Sb-W) deposit of Långban-type in Central Sweden, Mineral. Deposita, 36, 641–657, https://doi.org/10.1007/s001260100183, 2001.

Holtstam, D., Cámara, F., Karlsson, A., and Zack, T.: Jagoite revisited: crystal structure, mineral composition and paragenesis, Mineral. Mag., 89, 830–842, https://doi.org/10.1180/mgm.2025.10108, 2025.

Kampf, A. R., Pluth, J. J., Chen, Y. S., Roberts, A. C., and Housley, R. M.: Bobmeyerite, a new mineral from Tiger, Arizona, USA, structurally related to cerchiaraite and ashburtonite, Mineral. Mag., 77, 81–91, https://doi.org/10.1180/minmag.2013.077.1.08, 2013.

Magnusson, N. H.: Långbans malmtrakt, Sveriges Geol. Unders., Ser. Ca, 23, 1–111, 1930.

Mandarino, J. A.: The Gladstone–Dale compatibility of minerals and its use in selecting mineral species for further study, Can. Mineral., 45, 1307–1324, https://doi.org/10.2113/gscanmin.45.5.1307, 2007.

Mellini, M. and Merlino, S.: The crystal structure of jagoite, Am. Mineral., 66, 852–858, 1981.

Momma, K. and Izumi, F.: VESTA 3 for three-dimensional visualization of crystal, volumetric and morphology data, J. Appl. Crystallogr., 44, 1272–1276, https://doi.org/10.1107/S0021889811038970, 2011.

Moore, P. B.: Mineralogy & chemistry of Långban-type deposits in Bergslagen, Sweden, Mineral. Rec., 1, 154–172, 1970.

Ondruš, P., Veselovský, F., Gabašová, A., Hloušek, J., Šrein, V., Vavřín, I., Skála, R., Sejkora, J., and Drábek, M.: Primary minerals of the Jáchymov ore district, J. Czech Geol. Soc., 48, 19–147, 2003.

Sandström, F and Holtstam, D.: Geology of the Långban deposit. In: Långban. The mines, their minerals, geology and explorers.

Swedish Museum of Natural History and Raster Förlag, Stockholm, 29–41, ISBN 9789187214882, 1999.

Sheldrick, G. M.: SHELXT – Integrated space-group and crystal-structure determination, Acta Crystallogr. A, 71, 3–8, https://doi.org/10.1107/S2053273314026370, 2015a.

Sheldrick, G. M.: Crystal structure refinement with SHELXL, Acta Crystallogr. C, 71, 3–8, https://doi.org/10.1107/S2053229614024218, 2015b.

Skelton, A., Mansfeld, J., Ahlin, S., Lundqvist, T., Linde, J., and Nilsson, J.: A compilation of metamorphic pressure–temperature estimates from the Svecofennian province of eastern and central Sweden, GFF, 140, 1–10, https://doi.org/10.1080/11035897.2017.1414074, 2018.

Stephens, M. B. and Jansson, N. F.: Paleoproterozoic (1.9–1.8 Ga) syn-orogenic magmatism, sedimentation and mineralization in the Bergslagen lithotectonic unit, Svecokarelian orogen, in: Lithotectonic Framework, Tectonic Evolution and Mineral Resources, edited by: Stephens, M. B. and Bergman Weihed, J., Geol. Soc. London Mem., 50, https://doi.org/10.1144/M50-2017-40, 2020.